Applied Physics 应用物理, 2023, 13(5), 195-201
Published Online May 2023 in Hans. https://www.hanspub.org/journal/app
https://doi.org/10.12677/app.2023.135023

Hans汉斯

高阶非厄米系统的灵敏度研究

范孟军*，**付林雪**，**丁亚琼**，**付新铭**

上海理工大学理学院，上海

收稿日期：2023年3月28日；录用日期：2023年5月6日；发布日期：2023年5月12日

摘　要

我们提出了一个由三个无源谐振器组成的高阶系统的结构，近年来，相干完美吸收在各个方面受到越来越多的关注。相干完美吸收可以用于传感器的研究，我们将基于三态PT对称系统，通过分别对任何一个暗谐振器施加非本征扰动，我们可以清楚地观察到与微扰的立方根相关的频率响应。

关键词

非厄米系统，PT对称系统，奇异点，灵敏度

Study of the Sensitivity of High-Order Non-Hermitian System

Mengjun Fan*, **Linxue Fu**, **Yaqiong Ding**, **Xinming Fu**

College of Science, University of Shanghai for Science and Technology, Shanghai

Received: Mar. 28th, 2023; accepted: May 6th, 2023; published: May 12th, 2023

Abstract

We present the structure of a higher-order system consisting of three passive resonators, which have attracted increasing attention in recent years for coherent perfect absorption. Coherent perfect absorption can be used for the study of sensors, and we go over it based on a three-state PT symmetric system. The frequency response associated with the cubic root of the perturbation is clearly observed by applying a non-eigenetic perturbation to any of the dark resonators separately.

*通讯作者。

文章引用: 范孟军, 付林雪, 丁亚琼, 付新铭. 高阶非厄米系统的灵敏度研究[J]. 应用物理, 2023, 13(5): 195-201.
DOI: 10.12677/app.2023.135023

Keywords

Non-Hermitian System, PT Symmetry, Exceptional Point, Enhanced Sensitivity

1. 介绍

从量子力学的角度来看，如果一个量子系统与外部环境相连并引入了损耗，那么该系统就变成了一个开放的非厄米系统。同时，非厄米系统的概念可以应用于光学腔，这是近年来光学领域的一个热点。最近的研究表明，非厄米系统中的奇异点具有增强灵敏度[1] [2] [3] [4] [5]的巨大潜力。与厄米系统相比，非厄米系统可以完全改变系统的性质。体现这两个系统的差异的最好例子是奇异点的出现。所谓的奇异点是指两个或多个特征值及其特征态同时合并的点[6]。一些在光学系统中与奇异点有关的现象已经被证明，如拓扑手性[7] [8] [9] [10]、损失诱导透明[11] [12] [13] [14] [15]、单向不可见[16] [17]、功率振荡[18] [19] [20] [21]和激光[22] [23] [24] [25]。

相干完美吸收(CPA)是激光的时间反转过程，最初由 YD Chong 等人在 2010 年[26]提出。Sun 等人于 2014 年[27]首次在实验上观察到 PT 相变的相干完美吸收。相干完美吸收在许多领域都至关重要，如太阳能电池、隐身、检测和成像[28] [29] [30] [31]、超材料系统[32] [33] [34]、等离子体系统[35] [36] [37]和石墨烯系统[38] [39] [40] [41]，以及光子晶体[42] [43] [44] [45] [46]。

我们为了研究系统奇异点附近的灵敏度，通过改变此高阶系统的任意一个暗谐振器上加载的电容值来向系统施加非本征值扰动，通过观察在施加相同的扰动时 EP 点附近各自的频移去探究灵敏度。灵敏度的研究可以应用很多光学系统，如压力传感器或压力检测。

2. 理论与仿真

我们利用图 1 的结构研究了高阶非厄米系统的灵敏度，为了研究两个谐振器中的微小共振位移如何被影响，我们在两个谐振器上分别施加一个微扰 ε。通过调节谐振环 a 和谐振环 c 的电容值来添加微扰 ε。通过 CST 仿真软件进行模拟，然后确定合适的样品参数，整个样品的基板是介电常数为 2.2，厚度为 0.787 mm 的 RT5880 的双面覆铜介质板。微带线的宽度是 2.4 mm，两个 SRR 的总尺度分别为 8 mm × 8 mm，缝宽为 1 mm，线宽为 0.2 mm；从 SRR 到微带线的距离 10 mm。为了使结构更加紧凑，梳状线折叠成 U 形，梳状线的总长度为 62 mm，其中 h_1 = 25 mm；h_2 = 15 mm；h_3 = 22 mm；梳状线与谐振器 b 的耦合距离为 s_1，两个暗谐振器的耦合距离为 s_2，在仿真软件中调节耦合距离，使 $\tau = \eta = \kappa$；则 $s_1 = s_2$ = 0.2 mm。扰动加在谐振器 b 上和谐振器 c 上时的三态非厄米系统的耦合模方程如下：

$$\begin{aligned}
\frac{\mathrm{d}\tilde{a}}{\mathrm{d}t} &= \left(-iw_0 - \gamma_a - \Gamma_a\right)\tilde{a} - i\tau\tilde{b} + i\sqrt{2\gamma_a}\tilde{S}_{in} \\
\frac{\mathrm{d}\tilde{b}}{\mathrm{d}t} &= \left[-i\left(w_0 + \varepsilon\right) - \Gamma_a\right]\tilde{b} - i\tau\tilde{a} - i\eta\tilde{c} \\
\frac{\mathrm{d}\tilde{c}}{\mathrm{d}t} &= \left(-iw_0 - \Gamma_a\right)\tilde{c} - i\eta\tilde{b}
\end{aligned} \tag{1}$$

和

$$\begin{aligned}\frac{\mathrm{d}\tilde{a}}{\mathrm{d}t}&=\left(-iw_0-\gamma_a-\Gamma_a\right)\tilde{a}-i\tau\tilde{b}+i\sqrt{2\gamma_a}\tilde{S}_{in}\\ \frac{\mathrm{d}\tilde{b}}{\mathrm{d}t}&=\left[-iw_0-\Gamma_b\right]\tilde{b}-i\tau\tilde{a}-i\eta\tilde{c}\\ \frac{\mathrm{d}\tilde{c}}{\mathrm{d}t}&=\left(-i\left(w_0+\varepsilon\right)-\Gamma_c\right)\tilde{c}-i\eta\tilde{b}\end{aligned}\tag{2}$$

由(1)和(2)三态非厄米系统的哈密顿量可以分别写成：

$$H=\begin{pmatrix}w_0+i\left(\gamma_a-\Gamma_a\right) & \tau & 0\\ \tau & w_0+\varepsilon-i\Gamma_b & \eta\\ 0 & \eta & w_0-i\Gamma_c\end{pmatrix}\tag{3}$$

和

$$H=\begin{pmatrix}w_0+i\left(\gamma_a-\Gamma_a\right) & \tau & 0\\ \tau & w_0-i\Gamma_b & \eta\\ 0 & \eta & w_0+\varepsilon-i\Gamma_c\end{pmatrix}\tag{4}$$

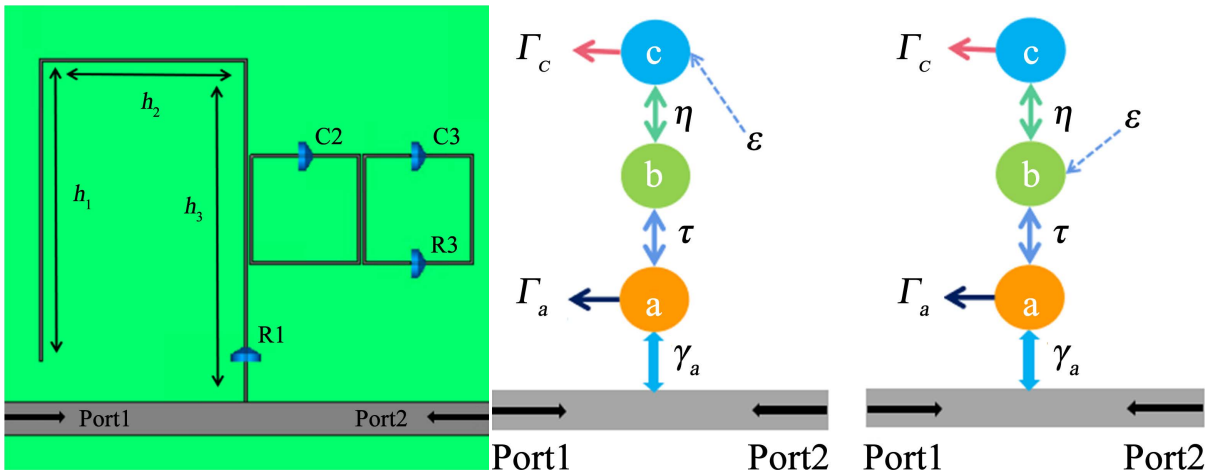

Figure 1. Structural model and theoretical model of the system
图 1. 系统的结构模型和理论模型

通过 CST 仿真软件对系统进行参数的拟合，得到系统的参数如下：亮态原子的散射损耗 $\gamma_a = 0.13$ GHz；亮态原子的耗散损耗 $\Gamma_a = 0.006R_1$；亮态原子的耗散损耗 $\Gamma_c = 0.009R_3$；三个谐振器均在 $w_0 = 0.91$ GHz 附近共振激发，两个暗谐振器 B 和 C 上的电容 $C_2 = C_3 = 2.74$ pf。利用[4]中的方法，对于谐振器 b 上的扰动，系统本征频率的实部位移近似为 $\mathrm{Re}\left(w_1\right)=w_0+2^{1/3}\kappa^{2/3}\varepsilon^{1/3}$，虚部总是零。对于谐振器 C 上的扰动，实部位移约为 $\mathrm{Re}\left(w_1'\right)=w_0-\kappa^{2/3}\varepsilon^{1/3}$，对应的虚部为 $\mathrm{Im}\left(w_1'\right)=\sqrt{2}/3\kappa^{1/3}\varepsilon^{2/3}$。图 2 展示了当微扰 ε 作用于谐振器 b 时，红色和黑色圆点分别是通过耦合模公式计算出的不同微扰作用在谐振器 b 上的 CPA 频移和谐振器 c 上的 CPA 频移，红色和黑色实线分别是通过近似实部和虚部公式计算时微扰作用在谐振器 b 上和谐振器 c 上的 CPA 频移。结果显示 dip 频移 $|\Delta w|\left(\Delta w=w_{\mathrm{dip}}-w_0\right)$ 与 $\mathrm{Re}\left(w_1\right)$ 完全一致。但对于谐振器 c 上的扰动，$\varepsilon > 0.08$ 时，位移 $|\Delta w'|\left(\Delta w'=w_{\mathrm{dip}}'-w_0\right)$ 明显偏离 $\mathrm{Re}\left(w_1'\right)$。如图 3 我们使用线性斜率(蓝色和紫色实线)更清楚的表明对数标度上的立方根行为。

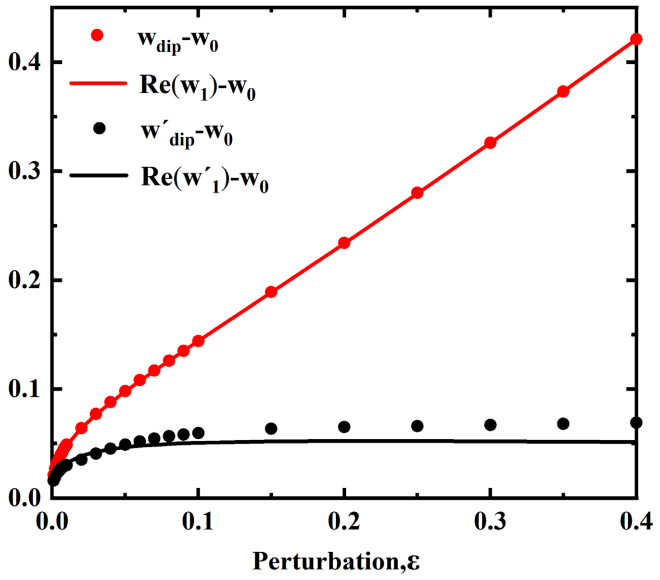

Figure 2. The difference between the calculated frequency shift of CPA and w_0 changes with the increase of ε
图 2. 计算的 CPA 的频移与 w_0 的差值随着 ε 的增加的变化

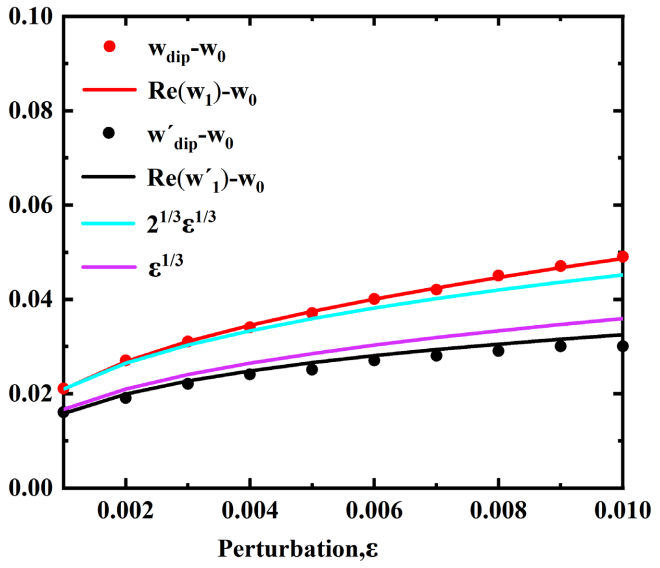

Figure 3. The result of (a) in logarithmic coordinates
图 3. 对数坐标上(a)的结果

3. 总结

我们通过耦合模方程得出系统的哈密顿量，进而推导出系统在加入微扰时相对于本征频率 w_0 的频移，再通过实虚部近似公式推导出系统在不同微扰下相对于本征频率 w_0 的频移，通过对比可以看出当扰动施加在中间的谐振器 b 上时，通过耦合模方程计算的频移与通过实虚部近似公式推导出的结果一致，但是当扰动施加在谐振器 c 上时，大于 0.08 时，通过耦合模方程计算的频移与通过实虚部近似公式推导出的结果明显发生偏移，并且通过观察在施加相同的扰动时各自的频移可以发现，在谐振器 c 施加扰动的灵敏度低于在在谐振器 b 施加扰动的灵敏度。我们的研究结果可能有助于实现受益于三阶例外点物理的无源无线传感系统的超灵敏度。

参考文献

[1] Wiersig, J. (2014) Enhancing the Sensitivity of Frequency and Energy Splitting Detection by Using Exceptional Points: Application to Microcavity Sensors for Single-Particle Detection. *Physical Review Letters*, **112**, Article ID: 203901. https://doi.org/10.1103/PhysRevLett.112.203901

[2] Chen, P.-Y. and Jung, J. (2016) PT-Symmetry and Singularity-Enhanced Sensing Based on Photoexcited Graphene Metasurfaces. *Physical Review Applied*, **5**, Article ID: 064018. https://doi.org/10.1103/PhysRevApplied.5.064018

[3] Lin, Z., Pick, A., Lončar, M. and Rodriguez, A.W. (2016) Enhanced Spontaneous Emission at Third-Order Dirac Exceptional Points in Inverse-Designed Photonic Crystals. *Physical Review Letters*, **117**, Article ID: 107402. https://doi.org/10.1103/PhysRevLett.117.107402

[4] Hodaei, H., Hassan, A.U., Wittek, S., Garcia-Gracia, H., El-Ganainy, R., Christodoulides, D.N. and Khajavikhan, M. (2017) Enhanced Sensitivity at Higher-Order Exceptional Points. *Nature*, **548**, 187-191. https://doi.org/10.1038/nature23280

[5] Chen, W., Özdemir, Ş.K., Zhao, G., Wiersig, J. and Yang, L. (2017) Exceptional Points Enhance Sensing in an Optical Microcavity. *Nature*, **548**, 192-196. https://doi.org/10.1038/nature23281

[6] Heiss, W.D. (2012) The Physics of Exceptional Points. *Journal of Physics A*: *Mathematical and Theoretical*, **45**, Article ID: 444016. https://doi.org/10.1088/1751-8113/45/44/444016

[7] Yin, C., Jiang, H., Li, L., *et al*. (2018) Geometrical Meaning of Winding Number and Its Characterization of Topological Phases in One-Dimensional Chiral Non-Hermitian Systems. *Physical Review A*, **97**, Article ID: 052115. https://doi.org/10.1103/PhysRevA.97.052115

[8] Leykam, D., Bliokh, K.Y., Huang, C., *et al*. (2017) Edge Modes, Degeneracies, and Topological Numbers in Non-Hermitian Systems. *Physical Review Letters*, **118**, Article ID: 040401. https://doi.org/10.1103/PhysRevLett.118.040401

[9] Jing, D.Y., Wang, H.Y. and Liu, W.M. (2022) Topological Transition and Majorana Zero Modes in 2D Non-Hermitian Chiral Superconductor with Anisotropy. *Journal of Physics*: *Condensed Matter*, **34**, Article ID: 195401. https://doi.org/10.1088/1361-648X/ac54e2

[10] Jin, L. and Song, Z. (2019) Bulk-Boundary Correspondence in a Non-Hermitian System in One Dimension with Chiral Inversion Symmetry. *Physical Review B*, **99**, Article ID: 081103. https://doi.org/10.1103/PhysRevB.99.081103

[11] Lü, H., Wang, C., Yang, L., *et al*. (2018) Optomechanically Induced Transparency at Exceptional Points. *Physical Review Applied*, **10**, Article ID: 014006. https://doi.org/10.1103/PhysRevApplied.10.014006

[12] Wang, C., Jiang, X., Zhao, G., *et al*. (2020) Electromagnetically Induced Transparency at a Chiral Exceptional Point. *Nature Physics*, **16**, 334-340. https://doi.org/10.1038/s41567-019-0746-7

[13] Zhang, H., Saif, F., Jiao, Y., *et al*. (2018) Loss-Induced Transparency in Optomechanics. *Optics Express*, **26**, 25199-25210. https://doi.org/10.1364/OE.26.025199

[14] Smith, D.D., Chang, H., Fuller, K.A., *et al*. (2004) Coupled-Resonator-Induced Transparency. *Physical Review A*, **69**, Article ID: 063804. https://doi.org/10.1103/PhysRevA.69.063804

[15] Qin, H., Ding, M. and Yin, Y. (2020) Induced Transparency with Optical Cavities. *Advanced Photonics Research*, **1**, Article ID: 2000009. https://doi.org/10.1002/adpr.202000009

[16] Huang, Y., Shen, Y., Min, C., *et al*. (2017) Unidirectional Reflectionless Light Propagation at Exceptional Points. *Nanophotonics*, **6**, 977-996. https://doi.org/10.1515/nanoph-2017-0019

[17] An, S., Liu, T., Liang, S., *et al*. (2021) Unidirectional Invisibility of an Acoustic Multilayered Medium with Parity-Time-Symmetric Impedance Modulation. *Journal of Applied Physics*, **129**, Article ID: 175106. https://doi.org/10.1063/5.0039432

[18] Rudnik, V.E., Ufa, R.A. and Malkova, Y.Y. (2022) Analysis of Low-Frequency Oscillation in Power System with Renewable Energy Sources. *Energy Reports*, **8**, 394-405. https://doi.org/10.1016/j.egyr.2022.07.022

[19] Valle, D.B. and Araujo, P.B. (2015) The Influence of GUPFC FACTS Device on Small Signal Stability of the Electrical Power Systems. *International Journal of Electrical Power & Energy Systems*, **65**, 299-306. https://doi.org/10.1016/j.ijepes.2014.10.012

[20] Kishor, N., Haarla, L., Seppänen, J., *et al*. (2013) Fixed-Order Controller for Reduced-Order Model for Damping of Power Oscillation in Wide Area Network. *International Journal of Electrical Power & Energy Systems*, **53**, 719-732. https://doi.org/10.1016/j.ijepes.2013.05.048

[21] Balasiu, F., Lazar, F.M. and Balaurescu, R. (2009) Defense Plan against Major Disturbances of the Romanian EPS. 2009 *IEEE Power & Energy Society General Meeting*, Calgary, 26-30 July 2009, 1-7. https://doi.org/10.1109/PES.2009.5275600

[22] Wagner, M., Ivleva, N.P., Haisch, C., *et al*. (2009) Combined Use of Confocal Laser Scanning Microscopy (CLSM) and Raman Microscopy (RM): Investigations on EPS-Matrix. *Water Research*, **43**, 63-76. https://doi.org/10.1016/j.watres.2008.10.034

[23] Kang, Y., Zhou, X.E., Gao, X., *et al*. (2015) Crystal Structure of Rhodopsin Bound to Arrestin by Femtosecond X-Ray Laser. *Nature*, **523**, 561-567. https://doi.org/10.1038/nature14656

[24] Schaffler, K., Nicolas, L.B., Borta, A., *et al*. (2017) Investigation of the Predictive Validity of Laser-EPs in Normal, UVB-Inflamed and Capsaicin-Irritated Skin with Four Analgesic Compounds in Healthy Volunteers. *British Journal of Clinical Pharmacology*, **83**, 1424-1435. https://doi.org/10.1111/bcp.13247

[25] Hassan, A.N., Frank, J.F. and Qvist, K.B. (2002) Direct Observation of Bacterial Exopolysaccharides in Dairy Products Using Confocal Scanning Laser Microscopy. *Journal of Dairy Science*, **85**, 1705-1708. https://doi.org/10.3168/jds.S0022-0302(02)74243-4

[26] Longhi, S. (2010) Backward Lasing Yields a Perfect Absorber. *Physics*, **3**, 61. https://doi.org/10.1103/Physics.3.61

[27] Sun, Y., Tan, W., Li, H., *et al*. (2014) Experimental Demonstration of a Coherent Perfect Absorber with PT Phase Transition. *Physical Review Letters*, **112**, Article ID: 143903. https://doi.org/10.1103/PhysRevLett.112.143903

[28] Pu, M., Feng, Q., Hu, C. and Luo, X. (2012) Perfect Absorption of Light by Coherently Induced Plasmon Hybridization in Ultrathin Metamaterial Film. *Plasmonics*, **7**, 733-738. https://doi.org/10.1007/s11468-012-9365-1

[29] Niesler, F.B.P., Gansel, J.K., Fischbach, S. and Wegener, M. (2012) Metamaterial Metal-Based Bolometers. *Applied Physics Letters*, **100**, Article ID: 203508. https://doi.org/10.1063/1.4714741

[30] Alves, F., Kearney, B., Grbovic, D. and Karunasiri, G. (2012) Narrowband Terahertz Emitters Using Metamaterial Films. *Optics Express*, **20**, 21025-21032. https://doi.org/10.1364/OE.20.021025

[31] Alves, F., Grbovic, D., Kearney, B., Lavrik, N.V. and Karunasiri, G. (2013) Bi-Material Terahertz Sensors Using Metamaterial Structures. *Optics Express*, **21**, 13256-13271. https://doi.org/10.1364/OE.21.013256

[32] Kang, M., Liu, F. and Li, J. (2013) Effective Spontaneous PT-Symmetry Breaking in Hybridized Metamaterials. *Physical Review A*, **87**, Article ID: 053824. https://doi.org/10.1103/PhysRevA.87.053824

[33] Baviskar, J., Mulla, A., Baviskar, A., *et al*. (2016) Metamaterial Lens Incorporated Enhanced Gain Omnidirectional Conformal Patch Antenna. 2016 *IEEE Aerospace Conference*, Big Sky, 5-12 March 2016, 1-7. https://doi.org/10.1109/AERO.2016.7500732

[34] Mavidis, C.P., Tasolamprou, A.C., Economou, E.N., *et al*. (2020) Polaritonic Cylinders as Multifunctional Metamaterials: Single Scattering and Effective Medium Description. *Physical Review B*, **102**, Article ID: 155310. https://doi.org/10.1103/PhysRevB.102.155310

[35] Jackson Jr., C., Reynolds, P.J. and Lindahl, I.L. (1975) Effect of Cyclophosphamide on Erythrocyte and Plasma Acetycholinesterase Activity in Sheep. *Journal of Animal Science*, **41**, 1390-1393. https://doi.org/10.2527/jas1975.4151390x

[36] Grossherr, M., Hengstenberg, A., Meier, T., *et al*. (2006) Discontinuous Monitoring of Propofol Concentrations in Expired Alveolar Gas and in Arterial and Venous Plasma during Artificial Ventilation. *The Journal of the American Society of Anesthesiologists*, **104**, 786-790. https://doi.org/10.1097/00000542-200604000-00024

[37] Spence, J.D., Malinow, M.R., Barnett, P.A., *et al*. (1999) Plasma Homocyst (e)ine Concentration, but Not MTHFR Genotype, Is Associated with Variation in Carotid Plaque Area. *Stroke*, **30**, 969-973. https://doi.org/10.1161/01.STR.30.5.969

[38] Luo, X., Cheng, Z.Q., Zhai, X., *et al*. (2019) A Tunable Dual-Band and Polarization-Insensitive Coherent Perfect Absorber Based on Double-Layers Graphene Hybrid Waveguide. *Nanoscale Research Letters*, **14**, Article No. 337. https://doi.org/10.1186/s11671-019-3155-z

[39] Sun, W., Wu, T., Wang, L., *et al*. (2019) The Role of Graphene Loading on the Corrosion-Promotion Activity of Graphene/Epoxy Nanocomposite Coatings. *Composites Part B*: *Engineering*, **173**, Article ID: 106916. https://doi.org/10.1016/j.compositesb.2019.106916

[40] Ning, Y., Dong, Z., Si, J., *et al*. (2017) Tunable Polarization-Independent Coherent Perfect Absorber Based on a Metal-Graphene Nanostructure. *Optics Express*, **25**, 32467-32474. https://doi.org/10.1364/OE.25.032467

[41] Ding, J., Zhao, H. and Yu, H. (2020) Superior to Graphene: Super-Anticorrosive Natural Mica Nanosheets. *Nanoscale*, **12**, 16253-16261. https://doi.org/10.1039/D0NR05040G

[42] Limpert, J., *et al*. (2004) All Fiber CPA System Based on Air-Guiding Photonic Bandgap Fiber Compressor. *Conference on Lasers and Electro-Optics*, San Francisco, 16-21 May 2004, 2.

[43] Sobon, G., Klimczak, M., Sotor, J., *et al*. (2014) Infrared Supercontinuum Generation in Soft-Glass Photonic Crystal Fibers Pumped at 1560 nm. *Optical Materials Express*, **4**, 7-15. https://doi.org/10.1364/OME.4.000007

[44] Ogino, J., Sueda, K., Kurita, T., *et al*. (2013) Development of High-Energy Fiber CPA System. *EPJ Web of Conferences*, **59**, Article No. 07004. https://doi.org/10.1051/epjconf/20135907004

[45] Wang, H., Kong, W., Zhang, P., *et al*. (2019) Coherent Perfect Absorption Laser Points in One-Dimensional Anti-Parity-Time-Symmetric Photonic Crystals. *Applied Sciences*, **9**, Article No. 2738. https://doi.org/10.3390/app9132738

[46] Ni, H., Zhou, G., Chen, X., *et al*. (2023) Non-Reciprocal Spatial and Quasi-Reciprocal Angular Goos-Hänchen Shifts around Double CPA-LPs in PT-Symmetric Thue-Morse Photonic Crystals. *Optics Express*, **31**, 1234-1248. https://doi.org/10.1364/OE.479595